NIH Public Access
Author Manuscript
J Nucl Med. Author manuscript; available in PMC 2012 December 26.

Published in final edited form as:
J Nucl Med. 2009 October ; 50(10): 1621–1630. doi:10.2967/jnumed.109.063982.

Quantitative analysis of myocardial perfusion SPECT anatomically guided by co-registered 64-slice coronary CT angiography

Piotr J. Slomka, PhD[1,2], **Victor Y. Cheng, MD**[1], **Damini Dey, PhD**[1,2], **Jonghye Woo, MSc**[1], **Amit Ramesh, MSc**[1], **Serge Van Kriekinge, PhD**[1,2], **Yasuzuki Suzuki**[1], **Yaron Elad, MD**[3], **Ronald Karlsberg, MD**[3], **Daniel S. Berman, MD**[1,2], and **Guido Germano, PhD**[1,2]

[1]Departments of Imaging and Medicine, Cedars-Sinai Medical Center, Los Angeles, CA

[2]Department of Medicine, David Geffen School of Medicine at UCLA, Los Angeles, CA

[3]Cardiovascular Medical Group, Beverly Hills, CA

Abstract

Aim—Sequential testing by coronary computed tomography angiography (CTA) and myocardial perfusion SPECT (MPS) obtained on standalone scanners may be needed to diagnose coronary artery disease (CAD) in equivocal cases. We have developed an automated technique for MPS-CTA registration and demonstrate its utility for improved MPS quantification by guiding the co-registered physiological (MPS) with anatomical CTA information.

Methods—Automated registration of MPS left ventricular (LV) surfaces with CTA coronary trees was accomplished by iterative minimization of voxel differences between pre-segmented CTA volumes and “motion-frozen” MPS data. Studies of 35 sequential patients (26 males), mean age 67±12 years with 64-slice coronary CTA, MPS and with available results of the invasive coronary angiography performed within 3 months were retrospectively analyzed. 3D coronary vessels and CTA slices were extracted and fused with quantitative MPS results mapped on LV surfaces and MPS coronary regions. Automatically co-registered CTA images and extracted trees were used to correct the MPS contours and to adjust the standard vascular region definitions for MPS quantification.

Results—Automated co-registration of MPS and coronary CTA had the success rate of 96% as assessed visually; the average errors were 4.3±3.3 mm in translation and 1.5±2.6 deg in rotation on stress and 4.2±3.1 mm in translation and 1.7±3.2 deg in rotation on rest. MPS vascular region definition was adjusted in 17 studies and LV contours were adjusted in 11 studies using co-registered CTA images as a guide. CTA-guided MP analysis resulted in improved area under the receiver operator characteristics (ROC) curves for the detection of RCA and LCX lesions as compared to standard MPS analysis 0.84±0.08 vs. 0.70±0.11 for LCX ($p = 0.03$) and 0.92±0.05 vs. 0.75±0.09 ($p=0.02$) for RCA.

Conclusions—Software image co-registration of standalone coronary CTA and MPS obtained on separate scanners can be performed rapidly and automatically allowing CTA-guided contour and vascular territory adjustment on MPS for improved quantitative MPS analysis.

Corresponding Author/ Reprint Requests: Piotr Slomka, PhD Cedars-Sinai Medical Center. Department of Imaging. #A047 8700 Beverly Blvd, Los Angeles, 90048, CA. USA. Piotr.Slomka@cshs.org Tel:1-310-423-4348 .

$watermark-text
$watermark-text
$watermark-text

Keywords

myocardial perfusion imaging; CT angiography; image registration; image fusion; coronary artery disease; image quantification

$watermark-text

$watermark-text

$watermark-text

INTRODUCTION

Recent advances in cardiac coronary CTA have allowed precise localization and classification of coronary artery plaques (1) as well as depiction of coronary anatomy. At the same time myocardial perfusion SPECT (MPS) continues to be a mainstream imaging modality for the detection and estimation of the severity of ischemia caused by coronary lesions. While either CTA or MPS will frequently produce adequate diagnostic information for the referring physician, a subset of patients undergoes sequential testing by both modalities due to inconclusive results obtained by one of the tests. (2, 3) In such cases, imaging results are often challenging to interpret due to presence of artifacts or equivocal findings in at least one modality.

It has been suggested that the visual analysis of fused MPS and coronary CTA images can synergistically improve the diagnostic value of sequential combined imaging (4), and manual tools for the purpose of combined visual analysis have been developed (5). However, the need for the interactive alignment complicates clinical protocols, introduces manual steps, and reduces practical usability of such tools. Furthermore, current coronary CTA image and MPS image fusion tools were proposed solely to improve subjective visual analysis and do not take advantage of the available CTA anatomic information, which can be used to refine quantitative MPS results.

In this work we aimed to develop a novel and practical tool for rapid automatic co-registration, visualization, and combined quantification of coronary CTA and MPS obtained from standalone scanners in different scanning sessions. Furthermore, we show that co-registered MPS/CTA data can be used to improve quantitative MPS analysis.

MATERIALS AND METHODS

Patient selection

Between 10/2005 and 05/2007, we identified retrospectively 40 consecutive patients who underwent myocardial MPS, CTA, and ICA within a 90-day period at Cedars-Sinai Medical Center (site A) or a neighboring outpatient imaging center (Cardiovascular Medical Group, Beverly Hills, California) (site B). The number of scans in which both CTA and MPS were performed was estimated at 5-10% of the MPS volume at both sites, and requiring ICA results further reduced eligible population in this study. For 2 patients the relevant imaging data could not be retrieved from the image archive and these cases were excluded. 22 patients were imaged for evaluation of symptoms (either chest pain or dyspnea, 8 had prior MI). The remaining 16 patients were asymptomatic and the imaging indications were for post-MI (3 cases) or post-PCI (3 cases) risk stratification and in 10 cases for risk stratification without prior event. Furthermore, 3 patients were excluded from further analysis because of coronary artery bypass graft surgery, which would present difficulty in assessing whether ischemia would be expected in the distribution of bypassed vessels in which regions subtended by proximal branch vessels may be ischemic despite open grafts to the distal vessel. The remaining 35 patients (26 men and 9 women; mean age 67±12 years) were included in our analysis. In 5 cases CTA and MPS were performed on the same day; in 20 cases CTA was performed after MPS (range 1-49 days, median 9 days); and in 10 cases MPS was performed after CTA (range 1-73 days, median 13 days). Table 1 contains patient

$watermark-text

$watermark-text

$watermark-text

characteristics. This study was approved by the Institutional Review Boards at Cedars-Sinai Medical Center and Cardiovascular Medical Group.

CT image acquisition

Since presence of coronary calcium can have significant effect on CTA image quality CT non contrast scans were performed and Agatston CT calcium scores obtained on ScImage workstation (Los Altos, California) (6, 7) (Site A) or SmartScore software (GE Healthcare) (Site B) . Coronary CTA was performed on the SOMATOM Definition dual-source CT (DSCT) scanner (Siemens Medical Systems, Forchheim, Germany) (Site A) or LightSpeed VCT 64-slice CT scanner (GE Healthcare, Waukesha, WI) (Site B*).* Pre-scan beta-blockade with a target heart rate of <60 beats/min (VCT) and < 70 beats/min (DSCT) and a non-contrast coronary calcium scan were performed. ECG-gated helical CTA was performed during a 9-12 second breath-hold by power-injecting 90-100 ml of intravenous contrast. Scanning parameters were: heart-rate dependent pitch, 0.33s (DSCT) to 0.35s (VCT) gantry rotation time, detector collimation of 0.625 mm, 120 kVp tube voltage and 300-700mAs tube current. ECG-based dose modulation 40-80% of the cardiac cycle was used to limit radiation dose.

Coronary CTA image reconstruction

Retrospectively-gated reconstruction of raw CTA data was performed at 40 to 80% of the R-R interval using the following parameters: 0.6-0.75 mm slice thickness, 250 mm field-of-view and 512×512 matrix. Coronary arterial trees were extracted from the best-quality phase using vendors' software and transferred to a Windows workstation for CTA-SPECT fusion.

CTA image evaluation

Coronary visual analysis was done with Circulation software packages (Siemens Medical Systems) and Advantage Workstation (Version 7.1, GE Healthcare). An experienced clinical coronary CTA reader (with > 300 previous coronary CTA interpretations), blinded to MPS and ICA results, assessed all coronary segments ≥ 1.5 mm in diameter by evaluating standard axial images, oblique multi-planar reformations, oblique maximum intensity projections, or centerline-based curved multi-planar reformations (8). Each segment was evaluated for presence and degree of stenosis. Any stenosis causing ≥ 50% or ≥ 70% luminal diameter narrowing by visual estimation were recorded. If a segment could not be assessed due to artifact, no stenosis was recorded.

ICA image acquisition and evaluation

ICA was performed with standard catheterization technique. All ICA used the same iodinated contrast (Visipaque, GE Healthcare). After ICA, a clinical interventional cardiologist, blinded to coronary CTA and MPS results, evaluated acquired images on an offline display station. For each coronary segment ≥ 1.5mm in diameter, this cardiologist determined by visual inspection whether ≥ 50% or ≥ 70% luminal diameter narrowing was present. For the purposes of comparison with MPS and CTA data, left main stenosis ≥50% was considered as significant for the left anterior descending artery and left circumflex artery (LCX) territories; the ramus intermedius vessel, if present, was assigned to the LCX territory. Angiographic findings are presented in Table 2.

Myocardial perfusion SPECT protocol

Studies were acquired at the 2 participating sites with the same dual isotope (Tl-Tc) protocol previously described (9). MPS acquisitions were performed with non-circular orbits, obtaining 64 projections over 180 degrees (45° RAO to 45° LPO). Acquisitions were performed on Philips CardioMD, Philips Forte, and Siemens e.cam cameras in one- or two-

day protocols. Stress scan was performed with exercise, adenosine injection, or adeno-walk protocol (10). All images were subject to standard clinical quality control measures, and all were reconstructed at a site B. No attenuation or scatter correction was used. Gated were reconstructed with filtered back projection (FBP) and with Butterworth filter (cut-off 0.83 cycles/cm, order 5) to original transverse orientation. Patients from Site A had 16-frame gated MPS and patients from Site B had 8-frame gated MPS.

Image processing

An overview of image processing is presented in Figure 1.

Motion frozen processing—Gated images were processed with "motion-frozen" algorithm as previously described (11) to provide static MPS images in end-diastolic (ED) phase to match the diastolic cardiac phase of coronary CTA. Briefly, in "motion-frozen" technique, derived LV contours (12-14) are used in combination with a thin-plate spline image warping (15).

Automated registration—The primary difficulty in accurate registration of MPS with coronary CTA is that different anatomic features appear on these images. Therefore, standard automated registration procedures (17), are prone to large errors. In particular, there could be severe perfusion defects present on MPS images that are not visualized in the myocardium on the CTA scan, which can present difficulties for generic registration algorithms. To provide a robust registration approach, we registered pre-segmented MPS volumes utilizing the left ventricular (LV) segmentation algorithm of QGS (14), combined with the additional segmentation of the blood pool region, derived from the MPS LV definition. In addition, to match cardiac phases between MPS and coronary CTA, we performed alignment of coronary CTA reconstructed in diastolic phases with segmented "motion frozen" slices of SPECT created from gated images. For both CTA and MPS, transverse image orientation is used during the registration process.

The MPS-CTA registration algorithm was implemented as follows. We initially align the center of mass of the segmented LV on MPS with the geometric center of the reconstructed coronary CTA image domain. Subsequently we perform iterative registration between CTA and segmented (LV, blood-pool) MPS images to find the transformation T that maps the source volume J(CTA) into correspondence with target volume I(MPS). We considered 6 rigid-body parameters for the MPS-CTA registration, assuming the cardiac phases are matched. Let S_I be segmented MPS volume which consists of blood pool, wall, and background regions. We used sum of squared differences (SSD) as a similarity measure and replaced the original MPS intensities with pre-assigned values for blood pool, myocardium and surrounding structures, which are derived from average HU values recorded by CTA in these regions. The proposed registration cost function E is given by

$$E(x, T(x)) = \int_{\Omega} (S_I(x + T(x)) - J^* G_\sigma(x))^2 dx,$$

where * denotes the convolution operator, and G_σ is Gaussian kernel with standard deviation σ and Ω is the image volume. We applied Gaussian filtering (with 3 mm kernel) to the CTA volume to suppress noise, and match image resolution to MPS. To minimize the cost function, we used iterative gradient descent and employed a coarse-to-fine multi-resolution scheme (3 levels) that helped to avoid local minima while achieving computational efficiency and robustness. We utilized the ITK registration libraries (18) for the implementation of the iterative registration. All algorithms were implemented in C++.

$watermark-text $watermark-text $watermark-text

$watermark-text

$watermark-text

$watermark-text

Validation of automatic registration—The automatic registration algorithm was assessed qualitatively and quantitatively for all 35 cases (total of 70 stress and rest datasets). Quantitative error analysis was performed by comparison to the expert manual alignment. The manual alignment parameters (3 translations and 3 rotations) were recorded for the comparison with the automated registration. Visual alignment was performed without the knowledge of the automatic results.

Vessel extraction and 3D visualization—For the 3D visualization of coronary vessels superimposed with MPS surfaces we utilized the processing information obtained from coronary CTA analysis on vendors' workstation. Subsequently, volume rendering was performed in OpenGL with the use of 2D/3D textures and pre-assigned color tables with varying RGB intensities and opacities to maximize the contrast opacity, provide realistic display (blood/tissue-pink/red, calcium-white) and minimize the influence of neighboring tissue such as fat (19).

Segmented CTA voxel maps could then be directly rendered in 3D with OpenGL methods within QPS and within the same coordinates as the epicardial 3D surface display with overlaid MPS function and perfusion information. We utilized level-of-detail rendering technique: high resolution image for final static display and a lower resolution during the user interaction and manipulation. In both cases, a 3D bounding box was used to speed-up the volume rendering of coronary arteries. The bounding box was directly computed from the coronary mask or from the coronary tree coordinates. The rendering was integrated with the standard 3D MPS epicardial surfaces. Raw perfusion information of quantitative blackout maps could be displayed on the epicardial surface. Stress and rest images had the same coronary CTA image superimposed. These segmented coronary trees derived from CTA were used only for display purposes and were not used in any way during the image registration process. Image registration algorithm was based only on the original transverse datasets.

MPS contour and territory adjustment—Fused coronary CTA and MPS images were evaluated with overlaid contours in multi-planar orientations (both cardiac axis and orthogonal views) in the fusion page of the QPS program. If discrepancies between the MPS valve plane position and the location on CTA could be seen on the fused images, contour adjustment was manually performed in the standard "Manual" QPS page with "Mask" and "Constrain" options and subsequently new contour was verified by the CTA fusion. Subsequently, the default vascular territory boundaries were overlaid with the 3D LV MPS surfaces, with color-coded perfusion information and with co-registered volume rendered segmented 3D coronary tree as described above. Vascular territories could then be adjusted segment-by-segment (based on a 17-segment American Heart Association model), utilizing anatomic information provided by the coronary CTA. If MPS contours or vascular territories needed to be adjusted based on the comparison with CTA, the quantitative MPS analysis was repeated with modified contours and territories.

CTA-guided MPS territory adjustment

MPS perfusion analysis was performed individually for each vessel with the use of the 'Group" function in QPS, in which 17 segments are assigned to a vascular territory based on the perfusion defect pattern (20, 21). The portion of the Total Perfusion Deficit (TPD) corresponding to a given territory was used for the automated quantification in each vessel, with the threshold of 2% as previously established (21). The MPS quantification results were recorded before and after adjustments based on the fused coronary data.

$watermark-text

$watermark-text

$watermark-text

Statistical Analysis

All continuous variables are expressed as mean ± one standard deviation. Paired t-tests were used to compare differences in paired continuous data and McNemar's tests were used to compare differences in paired discrete data. For unpaired continuous data, one-way ANOVA was used. All statistical tests were 2-tailed, and a value of $P < 0.05$ was considered significant. Receiver Operator Characteristics curves were constructed and compared using the Analyze-It 2.09 software (Leeds, UK) which implemented Delong-Delong method for ROC comparisons(22).

RESULTS

Out of 35 cases with all 3 scans (CTA, MPS, ICA) available, 20 patients underwent CTA after MPS and 15 underwent MPS after CTA. In cases in which CTA was performed after MPS, 11 had "equivocal" reversible defects on visual evaluation of MPS (interpreted as probably normal, borderline or probably abnormal), and 9 were referred to CTA because the care-taking physician felt defects seen on MPS were discordant with patient's clinical status or suspected multi-vessel disease. In cases in which patients underwent MPS after CTA, 7 had at least 1 non-diagnostic major coronary segment on CTA and 4 had maximal luminal stenosis in the LAD estimated at 50% and considered of borderline significance. Additionally, 4 patients were referred due to physician request to assess hypoperfusion by MPS after CTA scan.

Baseline findings

In the 35 cases studied, non-contrast CT calcium score was available in 33 cases. In these cases the average was 942±1530 (range 0 to 7781). Heavy calcification (score > 500) was present in 15 out of 33 datasets. In addition 10 cases demonstrated motion artifacts on CTA. Interpretation difficulties were noted in 9 cases. Presence of significant CT disease was noted in 27/35 studies, with 6 LCX lesions, 11 RCA lesions, 21 LAD lesions and 2 LM lesions.

MPS ejection fractions were 57.4%±14% (range from 32% to 83%) on stress and 57.2% ±14 (range 25% to 83%) on rest. Transischemic dilation (TID) was 1.15±0.14 (range 0.96-1.4). Visually, MPS scans were assessed as normal in 3 cases, as probably normal in 3 cases, borderline in 6 cases, probably abnormal in 1 case and abnormal in 22 cases. Quantitatively, total perfusion deficit (TPD) was 16.5±12.7% on stress (range 0 to 44%) and 5.6±8.1% on rest (range 0 to 25%).

Registration Algorithm

The execution speed of automated registration was approximately 1-2 seconds per study on a 3.0 GHz Pentium Dual Core computer. The automatic volume registration of "motion-frozen" MPS with CTA was successful in 33/35 stress and 34/35 rest studies as assessed qualitatively with an overall success rate of 96%. In one patient, due to the unusually high blood pool contrast intensity on coronary CTA, registration failed for both stress and rest study; the error occurred due to inadequate matching of assigned blood pool contrast with the actual CT value in the blood pool region. All 3 failed cases were female with small hearts (motion-frozen stress diastolic volumes 29-52ml on MPS). These results were easily corrected by interactive alignment. The quantitative registration errors obtained by comparison to the expert observer alignment are shown in Table 3. There were no significant differences between errors in different directions or between studies from 2 different systems. The errors ranged from 0 to 10 mm. Figure 2 shows an example of the fused images obtained by the automated co-registration of MPS with CTA.

$watermark-text

$watermark-text

$watermark-text

Contour and Territory Adjustments

MPS vascular region definitions were adjusted in 17 studies and LV contours (valve plane location) were adjusted in 11 studies using co-registered coronary CTA images as a guide. The territory adjustment modified perfusion results for a specific vessel but not the overall perfusion deficit per study. The MPS contour adjustment modified overall TPD perfusion results in 7/35 (20%) of the cases by more then 2%. The territory adjustments modified perfusion in a specific vessel but did not change the global perfusion measure per study.

Combined Performance for CAD detection

The areas under the ROC curve for the detection of disease in specific vessels are shown in Table 4, and corresponding ROC curves are shown in Figure 3. Sensitivities and specificities for detection of disease in LAD, LCX, and LAD arteries were 67%/50% 67%/83%, 67%/60% for MPS and 76%/71%, 75%/100%, 87%/85% for CTA-guided MPS respectively ($p = 0.025$ for RCA). CTA-guided MPS analysis correctly identified 17/21 LAD, 9/12 LCX, 13/15 RCA lesions corresponding to ≥70% stenosis on invasive angiography, compared to 17/21, 6/12, and 10/15 respectively by CTA alone and to 14/21, 8/12 and 10/15 by MPS quantification unaided by CTA. If a simple either/or (CTA or CTA-guided MPS) positive criterion was applied for detection of significant disease the number of detected lesions increased to 19/21 for LAD, to 10/12 for LCX, and 13/15 for RCA. Anatomic CTA-guided MPS reduced the number of discordant cases between CTA and quantitative MPS from 12 to 9 for the LAD, from 8 to 5 for LCX and from 12 to 6 for RCA. CTA-guided MPS agreed with angiography in 4/9 discordant cases for LAD, 4/5 cases for LCX and 3/6 for RCA.

In Figure 4, we show an example of MPS contour adjustment (valve plane position) based on MPS fusion. In Figure 5, we demonstrate an example of contour adjustment and territory adjustment which was performed after visual inspection of co-registered CTA/MPS images and quantitative MPS results obtained before and after these adjustments.

DISCUSSION

Software image fusion of coronary CTA and MPS has been proposed before to improve visual analysis of combined data from separate (4, 5) or hybrid scanners (23). Our work introduces several novel technical concepts related to this application, namely fully automatic registration, improvement of MPS quantification based on co-registered CTA and the use of motion-frozen MPS data. We demonstrated that accurate and robust automatic image registration of motion-frozen MPS and coronary CTA can be performed for data obtained on standalone scanners in as short as 1-2 seconds with a success rate of 96%. Previous studies of MPS-coronary CTA fusion required manual alignment of the image data (4, 5); it is likely that the automatic registration will allow of SPECT/CTA cardiac fusion in the clinical practice, whenever both datasets are available. We demonstrated that MPS contours – specifically the mitral valve plane position – can be adjusted based on the CTA anatomic volume data. Furthermore, we showed that the computerized MPS vascular region definitions can be modified based on co-registered coronary CTA anatomy and subsequently the quantitative results can be reassigned to the correct territories resulting in improved diagnostic performance especially for LCX and RCA lesions.

A previous report of clinical application for the CTA-MPS image fusion demonstrated that the correlation of stenosed segments with perfusion lesions allowed significant reduction of equivocal findings compared to side-by-side analysis of standalone CTA and MPS (4). In our work we show that CT-guided adjustment of contours and territories on MPS after image coregistration increases the diagnostic performance (area under the ROC curves) for detection of coronary disease. Further improvement in the overall accuracy, may be

$watermark-text

$watermark-text

$watermark-text

accomplished by a combined visual analysis scheme that takes into account the relative size and the severity of the stenosis and the presence of artifact on either of the two scans in a given location. When standalone CTA or MPS is insufficient to diagnose or localize CAD, CTA-guided MPS quantification can have an important role in increasing overall accuracy by lowering the number of discrepant findings. Since we studied a biased population with a high prevalence of equivocal results on the initial imaging test, we expect that the majority of the general MPS population will not significantly benefit from CTA-mediated contour and territory adjustments of MPS.

Although the automatic co-registration designed for coronary CTA and MPS volumes and CTA-guided MPS analysis have not been previously proposed, some related work has been reported. Faber et al. (24) developed a method of registration of 3D coronary anatomy reconstructed from invasive coronary angiography with MPS surfaces (24). They utilized a surface-to-point matching technique (25), which was modified to utilize coronary vessel information. Conceivably, such a registration approach could also be applied to the coronary CTA data; however, several of the arteries (RCA, left main) can be positioned some distance away from the myocardium, compromising the robustness of this approach. Furthermore, errors or branch omissions during vessel extraction could cause misregistration of the data. The use of volume data in our approach has the added advantage of allowing MPS contour verification by anatomic CTA volume (Figure 5), which would not be possible when only coronary tree data are co-registered. Others have previously proposed registration of MPS and non-contrast CT data obtained by the hybrid scanners for the purposes of attenuation correction (26); however in that application the data are already in an approximate alignment and only small correction is required. We have previously developed a MRI-MPS volume registration technique that utilized motion on MRI to pre-segment MRI heart for registration with MPS (27), but this approach could not be applied here since only one phase of the CTA data was available in this analysis. In addition, multi-phase data is not available for prospectively-gated CTA.

In this work we utilized “motion-frozen” MPS data (11) for the image registration with coronary CTA. “Motion-frozen” perfusion image corresponds to the ED phase of the cardiac cycle and therefore is better suited for fusion with coronary CTA, which is typically reconstructed in 70-80% phase for the visualization of the coronary lesions. In previous MPS-CTA fusion studies from standalone or hybrid scanners (4, 23), summed MPS data were utilized for image fusion. This could potentially lead to mismatches in the apparent size of the ventricle. “Motion-frozen” MPS images have end-diastolic myocardial dimensions and wall-thickness and therefore correspond more closely to CTA images.

The diagnostic results obtained for standalone CTA or MPS as shown in Figure 4 appear poor when compared to published reports on the respective performance of MPS and CTA modalities (21, 28). This is most likely due to the bias in our study population towards patients with frequent occurrences of equivocal results from the initial test and significant discrepancy between initial test interpretation and clinical suspicion. We demonstrated that, in such difficult cases, CTA-MPS image fusion and subsequent quantitative analysis can be helpful. Analysis of the diagnostic performance for specific vessels reveals that CTA-guided quantification was helpful in RCA and LCX territories, but did not significantly improve detection of LAD disease. This finding likely reflected the selective impact of basal contour adjustment on MPS.

This study analyzed the MPS-CTA data obtained by standalone scanners in two separate imaging sessions. Hybrid MPS-coronary CTA (29) or PET-coronary CTA imaging (30) performed in one session has been proposed for PET/CT scanners equipped with multislice CT. However, although hybrid dual-modality imaging has been established in oncology

$watermark-text

$watermark-text

$watermark-text

(31), it is not used routinely in cardiac imaging because of the difficulty in predicting "a-priori" which patients would benefit from such combined exam (32). Instead, a sequential approach is often applied in the clinical practice, with additional scans (CTA or MPS) performed only if the results of the initial modality are equivocal – as was the situation in our retrospective analysis. In addition, even if MPS-CTA scans are performed on a hybrid scanner, with data from both modalities in similar anatomic positions, software co-registration is still required due to mismatches in the respiratory phases (23). Since software registration can reliably bring MPS and CTA data acquired at different scanners into appropriate alignment as demonstrated in this work, the most practical approach for overall clinical effectiveness, minimization of the cost and radiation dose may be the sequential scanning as presented here, facilitated by software tools for automatic image registration and combined image analysis.

Mean estimated radiation dose from the CT scanning (CTA and coronary calcium scoring scan) was 19.7 mSv. For the dual-isotope stress-rest MPS scans, estimated radiation dose has been reported to be 24 mSv for injected radiopharmaceutical activity similar to our protocol (33). The two scans were not performed at the same time. Imaging teams at both sites have significantly reduced coronary CTA radiation dose by acquiring with prospective ECG-gating when possible (34, 35) and by using a patient-specific algorithm to select the optimal dose-lowering combination for retrospectively-gated acquisitions, with a resulting mean estimated CTA radiation dose of 2-5.8 mSv for prospective gating and 8 mSv for retrospective gating (34-36). Additionally, we have changed our standard MPS protocol to Tc-99m sestamibi for both stress and rest (estimated radiation dose for this protocol is 10 mSv) (33). Thus it is possible to perform a combined CTA and MPS study with the total dose < 20mSv even with CTA retrospective gating. It should be stressed that patients underwent either coronary CTA or stress-rest MPS first and only proceeded with dual scanning because of equivocal findings in the first scan or discrepancy between scan results and clinician assessment of patient status (typically in <10% of the total patient population).

This study has several limitations. Although we provided fully automated quantitative analysis and automated image registration, the contour definitions and vascular territory were manually-guided by the co-registered CTA anatomy; however it is feasible that this adjustment can be automated in the future if automatic segmentation of CTA scan is performed. The success of registration depends on successful MPS contour determination. If the contours are incorrectly determined, causing the LV shape to be grossly distorted, the automatic registration could fail. We performed the analysis in a retrospective fashion, and therefore data selection was biased by clinical conditions that led to performance of invasive angiography, MPS, and CTA, which occurs in a minority of patients undergoing evaluation for CAD. However, these data likely represent typical cases in which the CTA-guided MPS quantification could be clinically useful.

CONCLUSIONS

Software image co-registration of standalone coronary CTA and MPS obtained on separate scanners can be performed rapidly and automatically allowing CTA-guided contour and vascular territory adjustment on MPS for improved quantitative MPS analysis.

Acknowledgments

Cedars-Sinai Medical Center receives or may receive royalties for the licensure of software including software for quantitative assessment of myocardial perfusion and for MPS CT fusion, a portion of which is distributed to some of the authors of this manuscript (PS, SVK, DSB, GG).

$watermark-text
$watermark-text
$watermark-text

REFERENCES

1. Leber AW, Becker A, Knez A, et al. Accuracy of 64-slice computed tomography to classify and quantify plaque volumes in the proximal coronary system a comparative study using intravascular ultrasound. Journal of the American College of Cardiology. 2006; 47(3):672–677. [PubMed: 16458154]
2. Berman DS, Hachamovitch R, Shaw LJ, et al. Roles of Nuclear Cardiology, Cardiac Computed Tomography, and Cardiac Magnetic Resonance: Assessment of Patients with Suspected Coronary Artery Disease*. Soc Nuclear Med. 2006; Vol 47:74–82.
3. Hendel R, Patel M, Kramer C, Poon M, Carr JC, Gerstad NA. Appropriateness criteria for cardiac computed tomography and cardiac magnetic resonance imaging. J Am Coll Cardiol. 2006; 48(7): 1475–1497. [PubMed: 17010819]
4. Gaemperli O, Schepis T, Valenta I, et al. Cardiac image fusion from stand-alone SPECT and CT: clinical experience. J Nucl Med. May; 2007 48(5):696–703. [PubMed: 17475956]
5. Gaemperli O, Schepis T, Kalff V, et al. Validation of a new cardiac image fusion software for three-dimensional integration of myocardial perfusion SPECT and stand-alone 64-slice CT angiography. Eur J Nucl Med Mol Imaging. Jul; 2007 34(7):1097–1106. [PubMed: 17245532]
6. Agatston AS, Janowitz WR, Hildner FJ, Zusmer NR, Viamonte M, Detrano R. Quantification of coronary artery calcium using ultrafast computed tomography. Journal of the American College of Cardiology. 1990; 15(4):827–832. [PubMed: 2407762]
7. Berman DS, Wong ND, Gransar H, et al. Relationship between stress-induced myocardial ischemia and atherosclerosis measured by coronary calcium tomography. Journal of the American College of Cardiology. 2004; 44(4):923–930. [PubMed: 15312881]
8. Ferencik M, Ropers D, Abbara S, et al. Diagnostic Accuracy of Image Postprocessing Methods for the Detection of Coronary Artery Stenoses by Using Multidetector CT. Radiology. 2007; 243(3): 696. [PubMed: 17517929]
9. Berman DS, Kiat H, Friedman JD, et al. Separate acquisition rest thallium-201/stress technetium-99m sestamibi dual-isotope myocardial perfusion single-photon emission computed tomography: a clinical validation study. J Am Coll Cardiol. 1993; 22(5):1455–1464. [PubMed: 8227805]
10. Berman DS, Kang X, Hayes SW, et al. Adenosine myocardial perfusion single-photon emission computed tomography in women compared with men. Impact of diabetes mellitus on incremental prognostic value and effect on patient management. J Am Coll Cardiol. 2003; 41(7):1125–1133. [PubMed: 12679212]
11. Slomka PJ, Nishina H, Berman DS, et al. “Motion-Frozen” Display and Quantification of Myocardial Perfusion. J Nucl Med. Jul 1; 2004 45(7):1128–1134. 2004. [PubMed: 15235058]
12. Germano G, Kavanagh PB, Berman DS. An automatic approach to the analysis, quantitation and review of perfusion and function from myocardial perfusion SPECT images. Int J Card Imaging. 1997; 13(4):337–346. [PubMed: 9306148]
13. Germano G, Erel J, Lewin H, Kavanagh PB, Berman DS. Automatic quantitation of regional myocardial wall motion and thickening from gated technetium-99m sestamibi myocardial perfusion single-photon emission computed tomography. J Am Coll Cardiol. 1997; 30(5):1360–1367. [PubMed: 9350940]
14. Germano G, Kiat H, Kavanagh PB, et al. Automatic quantification of ejection fraction from gated myocardial perfusion SPECT. J Nucl Med. 1995; 36(11):2138–2147. [PubMed: 7472611]
15. Bookstein FL. Principal warps: thin-plate splines and the decomposition of deformations. IEEE Trans Pattern Anal Machine Intell. 1989; 11(6):567–585. 1989.
16. Slomka PJ, Dey D, Przetak C, Aladl UE, Baum RP. Automated 3-dimensional registration of stand-alone (18)F-FDG whole-body PET with CT. J Nucl Med. 2003; 44(7):1156–1167. [PubMed: 12843232]
17. Viola P, Iii WM Wells. Alignment by Maximization of Mutual Information. International Journal of Computer Vision. 1997; 24(2):137–154.
18. Ibáñez, L.; Schroeder, W.; Ng, L.; Cates, J. The ITK Software Guide. Kitware; 2003.

$watermark-text

$watermark-text

$watermark-text

19. Levin D, Aladl UE, Germano G, Slomka P. Techniques for Efficient, Real-Time, 3D Visualization of Multimodality Cardiac Data using Consumer Graphics Hardware. Comput Med Imaging Graph (submitted). 2004
20. Sharir T, Germano G, Waechter PB, et al. A new algorithm for the quantitation of myocardial perfusion SPECT. II: validation and diagnostic yield. J Nucl Med. 2000; 41(4):720–727. [PubMed: 10768575]
21. Slomka PJ, Nishina H, Berman DS, et al. Automated Quantification Of Myocardial Perfusion SPECT Using Simplified Normal Limits. J Nucl Cardiol. 2005; 12(1):66–77. [PubMed: 15682367]
22. DeLong ER, DeLong DM, Clarke-Pearson DL. Comparing the areas under two or more correlated receiver operating characteristic curves: a nonparametric approach. Biometrics. 1988:837–845. [PubMed: 3203132]
23. Rispler S, Keidar Z, Ghersin E, et al. Integrated single-photon emission computed tomography and computed tomography coronary angiography for the assessment of hemodynamically significant coronary artery lesions. J Am Coll Cardiol. Mar 13; 2007 49(10):1059–1067. [PubMed: 17349885]
24. Faber TL, Santana CA, Garcia EV, et al. Three-Dimensional Fusion of Coronary Arteries with Myocardial Perfusion Distributions: Clinical Validation. J Nucl Med. May 1; 2004 45(5):745–753. 2004. [PubMed: 15136621]
25. Besl P, McKay N. A method for registration of 3D shapes. IEEE Trans Pattern Anal Machine Intell. 1992; 14:239–256.
26. Guetter C, Wacker M, Xu C, Hornegger J. Registration of Cardiac SPECT/CT Data Through Weighted Intensity Co-occurrence Priors. LECTURE NOTES IN COMPUTER SCIENCE. 2007; 4791:725.
27. Aladl UE, Hurwitz GA, Dey D, Levin D, Drangova M, Slomka PJ. Automated Image Registration of Gated Cardiac Single-Photon Emission Computed Tomography and Magnetic Resonance Imaging. J Magn Reson Imaging. 2004; 19(3):283–290. [PubMed: 14994295]
28. Delago A, Min JK, Halamert E, et al. Diagnostic Performance of 64-Multidetector Row Coronary Computed. Journal of the American College of Cardiology.
29. Rispler S, Keidar Z, Ghersin E, et al. Integrated Single-Photon Emission Computed Tomography and Computed Tomography Coronary Angiography for the Assessment of Hemodynamically Significant Coronary Artery Lesions. Journal of the American College of Cardiology. 2007; 49(10):1059–1067. [PubMed: 17349885]
30. Di Carli MF, Dorbala S, Hachamovitch R. Integrated cardiac PET-CT for the diagnosis and management of CAD. J Nucl Cardiol. 2006; 13(2):139–144. [PubMed: 16580946]
31. Townsend DW. Dual-Modality Imaging: Combining Anatomy and Function. J Nucl Med. 2008; 49(6):938. [PubMed: 18483101]
32. Slomka PJ, Berman DS, Germano G. Applications and software techniques for integrated cardiac multimodality imaging. Expert Review of Cardiovascular Therapy. 2008; 6(1):27–41. [PubMed: 18095905]
33. Einstein AJ. Radiation risk from coronary artery disease imaging: how do different diagnostic tests compare? Heart. Dec; 2008 94(12):1519–1521. [PubMed: 19011135]
34. Gutstein A, Wolak A, Lee CJ, Dey D, Ohba M, Suzuki Y, Cheng V, Gransar H, Suzuki S, Friedman JD, Thomson LEJ, Hayes S, Pimentel R, Paz W, Slomka PJ, Berman DS. Predicting success of prospective and retrospective gating with dual-source coronary computed tomography angiography: Development of selection criteria and initial experience. Journal of Cardiovascular Computed Tomography. 2008; 2:81–90. [PubMed: 19083926]
35. Gopal A, Mao SS, Karlsberg D, et al. Radiation reduction with prospective ECG-triggering acquisition using 64-multidetector Computed Tomographic angiography. Int J Cardiovasc Imaging. Apr; 2009 25(4):405–416. [PubMed: 19051055]
36. Gutstein A, Dey D, Cheng V, Wolak A, Gransar H, Suzuki Y, Friedman J, Thomson LEJ, Hayes S, Pimentel R, Paz W, Slomka P, Le Meunier L, Germano G, Berman DS. Algorithm for radiation dose reduction with helical dual source coronary computed tomography in clinical practice. Journal of Cardiovascular Computed Tomography. 2008; 2:311–322. [PubMed: 19083968]

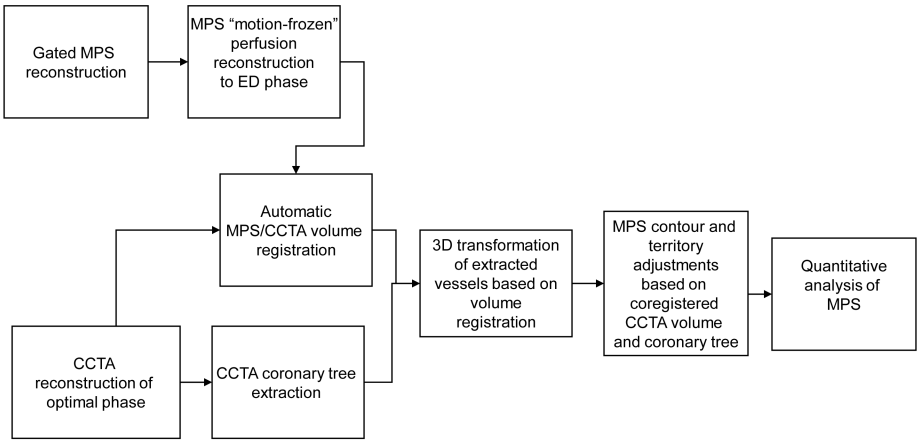

Figure 1.
Overview of image processing.

$watermark-text
$watermark-text
$watermark-text

$watermark-text

$watermark-text

$watermark-text

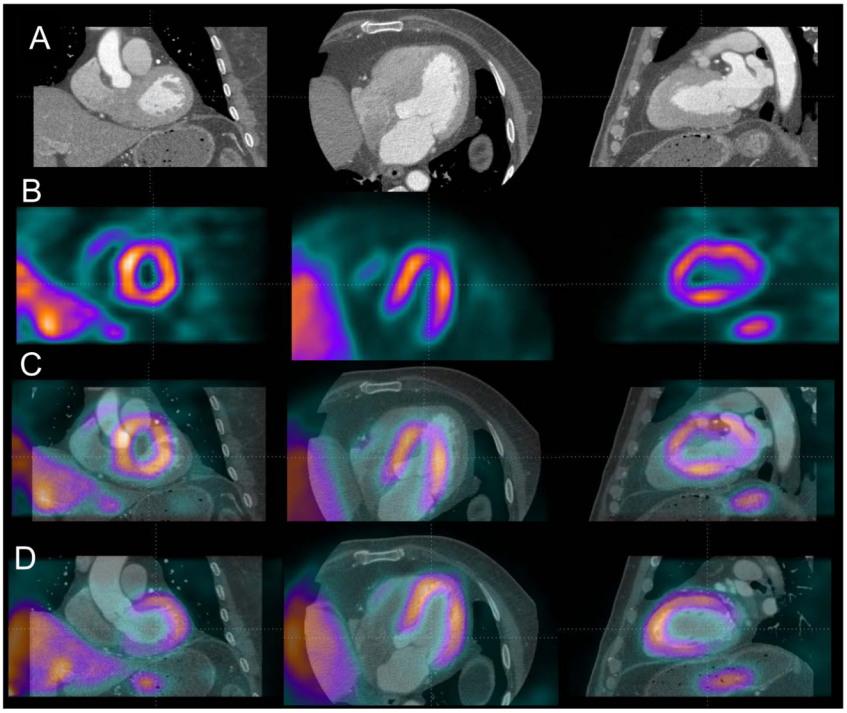

Figure 2.
Automated volume alignment of CTA and MPS. In 4 rows from top to bottom we show in multi-planar orientations original CTA images (A), original MPS images (B), fused unregistered MPS and CTA images (C) and the same images after automated volume registration (D). Subsequently, the 3D transformation parameters obtained from the volume registration can be used to align associated coronary trees with MPS surfaces.

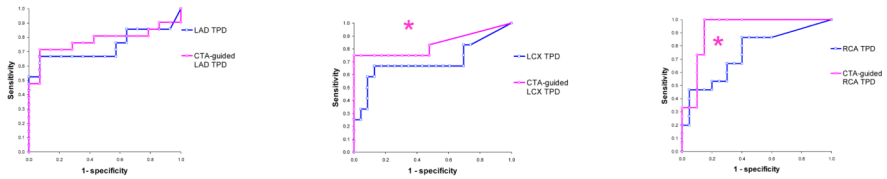

Figure 3.
ROC curves for the disease detection in individual vessels by partial Total Perfusion Deficit per vessel in standalone MPS (blue) and CTA-guided MPS (pink) for LAD (Left), LCX (Middle) and RCA (Right) vascular territories.

$watermark-text
$watermark-text
$watermark-text

$watermark-text

$watermark-text

$watermark-text

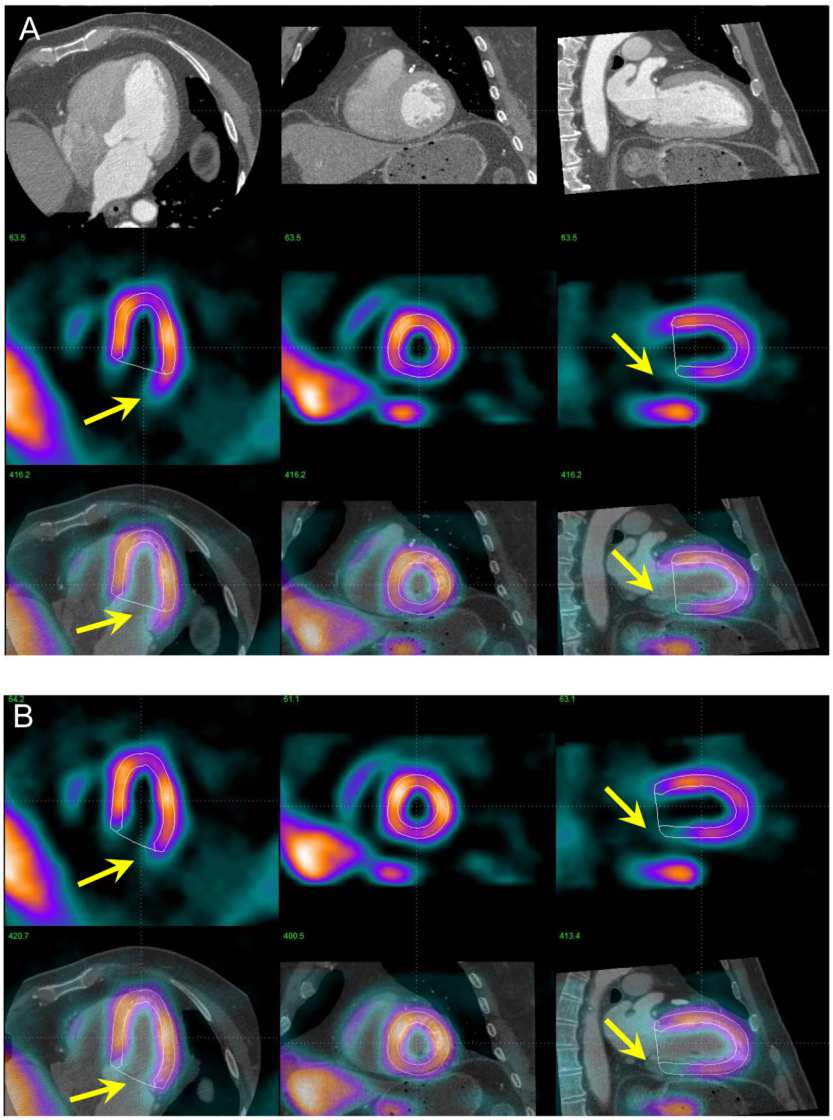

Figure 4.
Example of MPS contour adjustment after MPS-CTA coregistration. In panel A, co-registered CTA and MPS images are shown in the same configuration as in Figure 2 with MPS contours overlaid (white lines). Image fusion reveals that the valve plane is determined incorrectly (yellow arrows). The same images are shown after MPS contour adjustment (B), revealing RCA defect on MPS. ICA confirmed a ≥ 70% stenosis in the RCA.

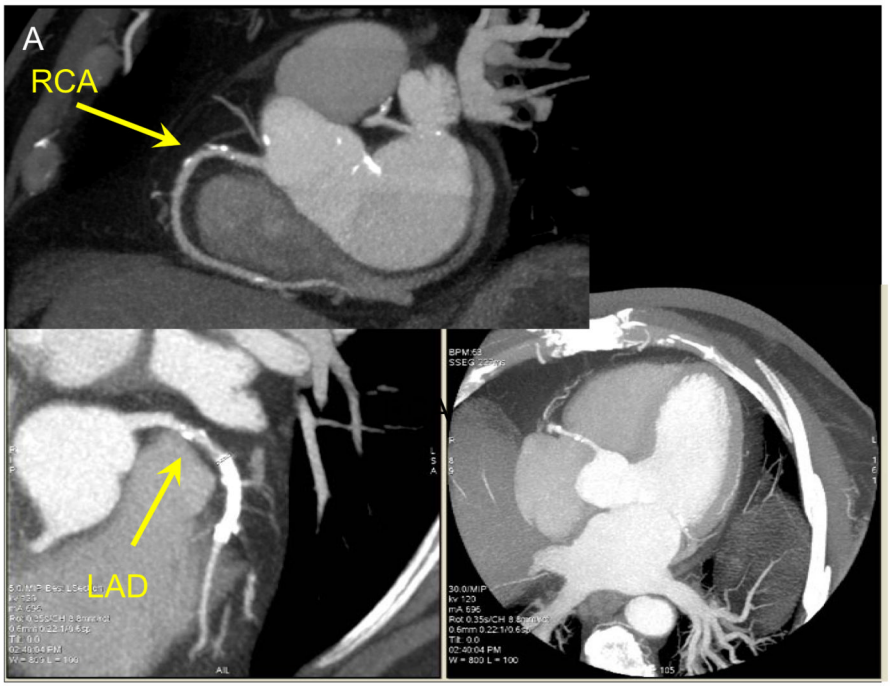

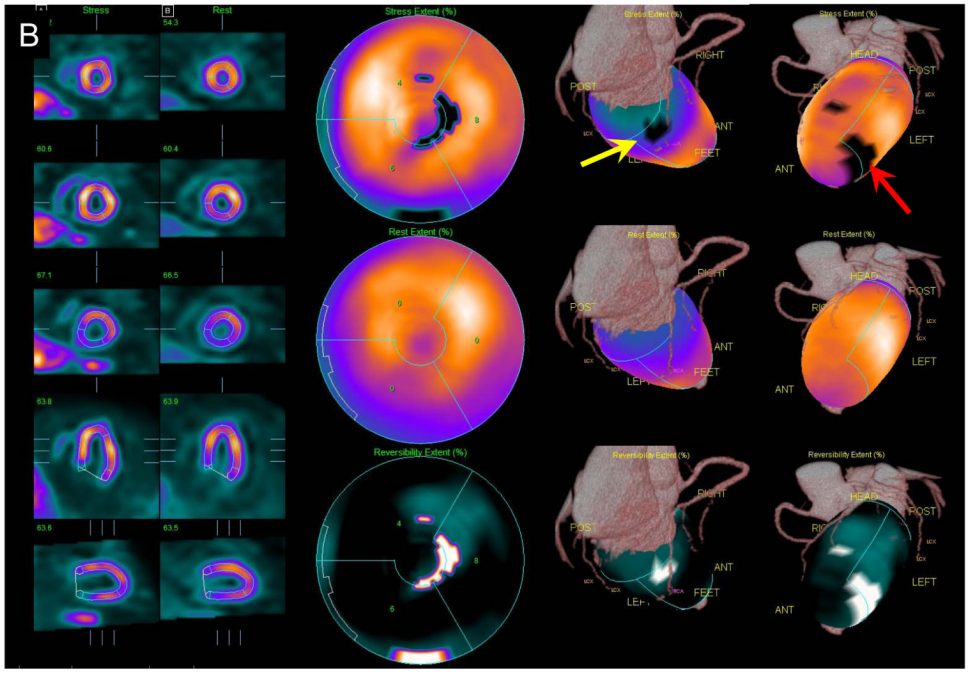

$watermark-text
$watermark-text
$watermark-text

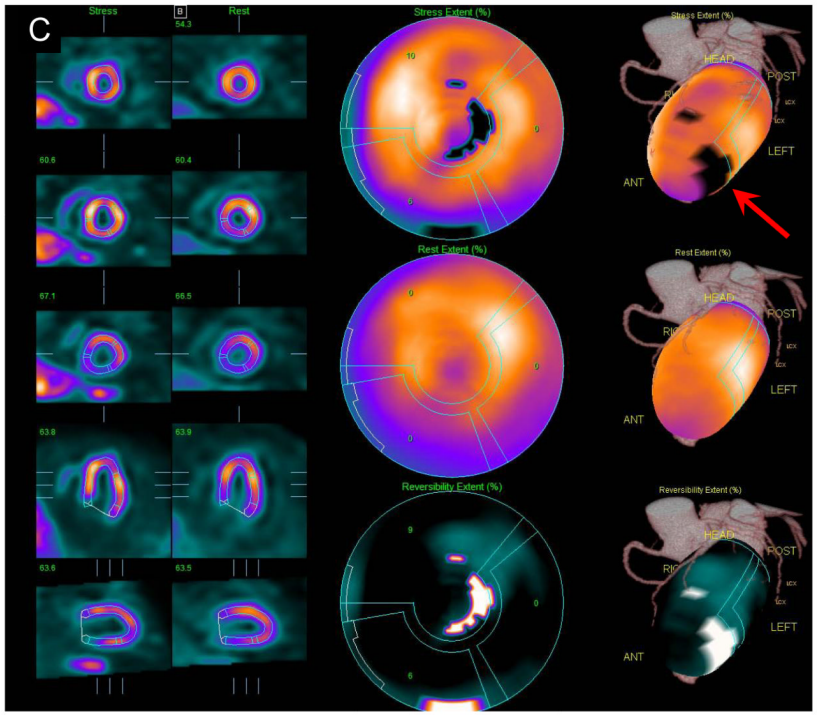

Figure 5.

Example of MPS contour and territory adjustment based on CTA in a 72 y/o male patient. Original coronary CTA images (A) were interpreted to show a non-significant, <50% proximal RCA lesion and significant LAD lesion. Coregistration of CTA and MPS images was performed and indicated the need for contour adjustment (as shown in Figure 4). Quantification after contour adjustment reveals a 3% defect in the typical RCA territory (yellow arrow) and defect between LAD and LCX (red arrow) (B). After adjustments of the coronary territory based on the superimposed CTA coronary tree the MPS lesion is assigned to LAD (C). ICA revealed a 50-69% RCA lesion and a 90% LAD lesion. In this case CTA-guided analysis allowed identification of the additional RCA lesion in MPS and reassignment of the second defect from LAD/LCX to LAD.

$watermark-text
$watermark-text
$watermark-text

$watermark-text

$watermark-text

$watermark-text

Table 1

Characteristics of patients.

Parameter	Mean Value
Gender Male (%)	26 (74%)
Age (years)	67±12 years
Asymptomatic	15 (43%)
Myocardial Infarction	11 (31%)
Weight	80±16kg
Body Mass Index	27.6±5.7

$watermark-text

$watermark-text

$watermark-text

Table 2

Angiographic characteristics of data (n=35).

Parameter	Value/(%)
≥70% stenosis	27/(77%)
≥ 50% stenosis	32/(91%)
Left Main ≥ 50% stenosis	6/(17%)
LAD (≥70%)	21 (60%)
LCX (≥70%)	12 (34%)
RCA (≥70%)	15 (43%)
No stenosis ≥50%	3 (9%)
No stenosis ≥70%	8 (23%)
1 vessel disease (≥70%)	11 (31%)
2 vessel disease (≥70%)	11 (31%)
3 vessel disease (≥70%)	5 (14%)

$watermark-text

$watermark-text

$watermark-text

Table 3

Areas under the ROC curves (AUC-ROC) for the detection of the CAD (≥ 70% luminal stenosis) in the individual vessels by standard quantitative MPS, CTA, and anatomically-guided MPS.

AUC-ROC	LAD	LCX	RCA
MPS	0.74±0.08	0.70±0.11	0.75±0.09
CTA	0.76±0.09	0.75±0.09	0.81±0.07
CTA-guided MPS	0.78±0.08	0.84±0.08 *	0.92±0.05 *

* significantly different than MPS

$watermark-text $watermark-text $watermark-text

Table 4

Accuracy of automated alignment of SPECT and coronary CTA for translations and rotations (n=35 for each rest and stress).

	Translations [mm]			Rotations [deg]		
	X	**Y**	**Z**	**XY**	**XZ**	**YZ**
Rest	4.1±3.5	4.0±3.6	3.0±2.5	2.4±3.5	1.4±3.3	1.3±2.6
Stress	4.4±3.3	4.4±3.4	3.4±2.4	2.3±3.3	1.2±3.0	1.7±3.2

J Nucl Med. Author manuscript; available in PMC 2012 December 26.